NASA TECHNICAL NOTE

NASA TN D-5576

C. 1

TECH LIBRARY KAFB, NM
0132366

NASA TN D-5576

LOAN COPY: RETURN TO
AFWL (WLOL)
KIRTLAND AFB, N MEX

DISTRIBUTION OF NEUTRAL PROPELLANT FROM ELECTRIC THRUSTERS ONTO SPACECRAFT COMPONENTS

by Thaine W. Reynolds and Edward A. Richley

Lewis Research Center
Cleveland, Ohio

NATIONAL AERONAUTICS AND SPACE ADMINISTRATION • WASHINGTON, D. C. • DECEMBER 1969

TECH LIBRARY KAFB, NM
0132366

1. Report No. NASA TN D-5576	2. Government Accession No.	3. Recipient's Catalog No.
4. Title and Subtitle DISTRIBUTION OF NEUTRAL PROPELLANT FROM ELECTRIC THRUSTERS ONTO SPACECRAFT COMPONENTS		5. Report Date December 1969 6. Performing Organization Code
7. Author(s) Thaine W. Reynolds and Edward A. Richley		8. Performing Organization Report No. E-4810
9. Performing Organization Name and Address Lewis Research Center National Aeronautics and Space Administration Cleveland, Ohio 44135		10. Work Unit No. 120-26 11. Contract or Grant No.
12. Sponsoring Agency Name and Address National Aeronautics and Space Administration Washington, D.C. 20546		13. Type of Report and Period Covered Technical Note 14. Sponsoring Agency Code

15. Supplementary Notes

16. Abstract

Calculations based on proposed models of two Jupiter flyby probes indicated high enough neutral mercury fluxes on solar panels that condensation could occur halfway through the mission thrusting period. Return fluxes to spacecraft surfaces, while lower, may also encounter condensing conditions because of the possible lower temperature of such surfaces. A simple procedure is presented for estimating possible neutral propellant flux onto surfaces downstream of an electric thruster, or, through reflection or desorption, onto spacecraft surfaces upstream of the thruster exhaust plane.

17. Key Words *(Suggested by Author(s))* Electric propulsion Mercury (metal) Solar panels Condensation	18. Distribution Statement Unclassified - unlimited

19. Security Classif. (of this report)	20. Security Classif. (of this page)	21. No. of Pages	22. Price*
Unclassified	Unclassified	36	$3.00

*For sale by the Clearinghouse for Federal Scientific and Technical Information Springfield, Virginia 22151

DISTRIBUTION OF NEUTRAL PROPELLANT FROM ELECTRIC THRUSTERS ONTO SPACECRAFT COMPONENTS*

by Thaine W. Reynolds and Edward A. Richley

Lewis Research Center

SUMMARY

The problem of neutral propellant atom fluxes arriving at surfaces situated near the exhaust of ion thrusters is considered. The problem is of interest because, for some interplanetary missions, the combination of long thrusting times and low surfaces temperatures allows ample opportunity for the buildup of an adsorbed layer of propellant. Both the thermal and electrical behavior of solar panel arrays are affected by such a layer. Even spacecraft component surfaces outside a line of sight to the thruster exhaust may receive propellant impingement through reflection or reevaporation from line-of-sight surfaces.

Neutral mercury flux rates onto the solar panels of two different designs of proposed Jupiter flyby probes were estimated to be in the range of 100 to 500 equivalent monolayers per day over portions of the panel closest to the thrusters. With these flux levels, condensation of mercury can occur on the panels in the latter stages of the mission, specifically when the spacecraft is at a range of about 1.7 to 2.0 astronomical units. And, as the mission proceeds, condensation can occur over portions of the panel which extend outward away from the thruster.

The possible importance of solar panel temperature history is also described. It is shown that an unplanned for, premature, cooling of the panel could upset the thermal equilibrium sufficiently that propellant condensation can occur. The condensate might reevaporate or condensation might then continue, depending on which surfaces were affected.

*Portions of this report were presented at the AIAA Seventh Electric Propulsion Conference, Williamsburg, Va., Mar. 3-5, 1969. (AIAA Paper No. 69-270.)

INTRODUCTION

In designing a solar-electric spacecraft, one area of concern is that of determining the effects of the thruster propellant exhaust on various spacecraft components, such as solar cell panels, power conditioning units, telemetry gear, or other instrumentation. At first thought, it may appear that the problem is easily avoided by simply locating the thrusters on the spacecraft so that the thruster exhaust has no direct line of sight to any of the spacecraft components. However, constraints imposed by conventional packaging and deployment methods may make this design approach impractical.

Exhausts from electrostatic thrusters consist of the highly energetic charged particles of the ion beam, lower energy charge-exchange ions, and low energy neutral particles (fig. 1). The latter are the result of thruster inefficiencies. Each type of thruster propellant efflux presents a different interaction problem potential.

To date only a few studies dealing with expected impingement rates of propellant upon surfaces of a spacecraft have appeared in the literature. Backflow from high pressure gaseous jet exhausts has been considered (refs. 1 and 2). The potential impingement problem with respect to ion beams has been recognized (refs. 3 and 4). The specific effects of such impingement rates on particular surfaces is the subject of other investigations (ref. 4). Finally, experimental determination of the possible effects of mercury contamination on clean surfaces is planned for a forthcoming SERT flight (ref. 5).

The high energy primary exhaust particles are capable of causing severe erosion of objects in their path. Clearly, this type of encounter must be avoided. Fortunately, in most electric thruster types, the high energy exhaust particles are reasonably well collimated. For example, it has been determined from a study of exhaust beam profile maps from several mercury ion thrusters at the Lewis Research Center that over 96 percent of the primary ion beam is confined within a beam spreading half-angle of 20° (fig. 2). Thus, most interactions of this kind can be avoided by simply designing the spacecraft to permit a clear exhaust area for the main beam over these spreading angles.

Charge-excharge ions formed in the exhaust beam are not collimated, and impaction on surrounding surfaces could be a problem. However, both the quantity and energy levels are considerably less than those of the primary ions (ref. 3). The charge-exchange ion flux is also much lower than the neutral mercury atom flux (ref. 3) and the directional distribution is a complex function of the electric fields existing at the point of creation.

Because of the magnitude of neutral efflux and the lack of collimation, neutral particle effluxes present a potentially serious problem. These particles leave the thruster with essentially a cosine distribution (ref. 6); that is, particle flux in a given direction

is proportional to the cosine of the angle made with the beam axis. Some will arrive at and become deposited on any component surface located downstream of the thruster exhaust plane. Furthermore, these particles will also be reflected or desorbed from such downstream surfaces and some may arrive at spacecraft component surfaces upstream of the thruster exhaust plane - surfaces that are otherwise free from any primary particle impingement.

If under the thermal conditions of the surface, the arrival (or condensation) rates exceed the possible desorption rates, component performance might be seriously affected by cumulative propellant deposits. For example, metallic propellants such as cesium, mercury, or lithium may result in degradation of performance of solar cell arrays due to effects on optical properties or electrical failures. If rapid chemical reaction between the propellant and surface is possible, deleterious effects might occur even without cumulative condensation. It is possible that monolayer coverage of the propellant gas on the surface may be reached relatively quickly, but subsequent layers will not build up. It is therefore of some consequence to know whether the phenomenon associated with the adsorbing species and a particular surface is of importance at monolayer concentrations. Many surface properties, such as work function, ion emission rate, surface diffusion, catalytic reactions, and electrical conductivity, to name a few, are strongly affected by such low-level concentrations. Other properties, such as light transmission or thermal emittance also may be affected at low-level surface concentrations.

Each design of a spacecraft requires a specific calculation of the possible propellant impingement rates. However, some simple general calculations will show whether the magnitude of the impingement is sufficient to warrant more detailed consideration. Similarly, the relations involved in the determination of surface coverage are relatively simple and general calculations involving these parameters may be made. Detailed calculations pertaining to a particular application, thus, may not be necessary.

With these thoughts in mind, this report presents:

(1) General calculations of particle arrival rates at planes located downstream of a source

(2) Calculations of reflected or reevaporated particle flux back toward the source (or thruster) plane

(3) Desorption rates of adsorbed gas layers in terms of desorption energies and surface temperatures

(4) An illustration of applications of the general calculations to two different configurations of proposed Jupiter flyby probe designs (refs. 7 and 8)

ANALYSIS

The process of condensate formation on a surface is a competition between the rate at which particles arrive and stick, and the rate at which they can leave the surface; that is,

$$\frac{d\sigma}{dt} = \mu S - \nu_d$$

where

σ surface concentration of adsorbed species

μ arrival rate

S sticking coefficient

ν_d desorption rate

(All symbols are defined in appendix A.)

The arrival rate μ depends on the strength of the source of particles, the distance of the surface from the source, and on the orientation of the surface with respect to the direction of the incoming particles. Arrival rates thus depend on geometric relations as well as the factors governing the strength of the source of particle emission. In the flux calculations herein, free-molecule flow conditions are assumed to prevail. The sticking coefficient is assumed to be 1 for convenience. However, for any situation where it is not 1, it may be easily carried along in the calculations.

The desorption rate ν_d depends most strongly on the temperature of the surface and the desorption energy - the strength of the bond between the adsorbed particles and the surface. If the "surface" happens to be the same material as the adsorbing gas, the desorption energy is simply the sublimation energy. The desorption energy of a gas from a surface other than itself may be considerably different from the sublimation energy of the gas.

Arrival Rates

The coordinate system that is used in this analysis is shown in figure 3. In general, the particle source may be located arbitrarily at point (a, b, c). The primary surface of interest on which particles may condense is located downstream of the exit plane of the thrusters. Arrival flux is calculated at a general point (x, y, z) in this plane. Surfaces upstream of the exit plane of the thruster may also be impinged on, and these surfaces will be referred to as secondary surfaces.

Primary surfaces. - The ratio of the arrival rate μ at a surface to the emission rate ν from a point source emitting diffusely under conditions of free-molecule flow is given by (ref. 9):

$$\frac{\mu}{\nu} = \frac{\cos \alpha_1 \cos \alpha_2}{\ell^2} \tag{1}$$

All length variables herein are dimensionless ratios with respect to the thruster radius. Otherwise, any consistent set of units may be used. Equation (1) is a point source relation. However, it is readily shown that it yields fluxes that are within 5 percent of the more exact disk source relation at locations as close as 5 source radii away (ref. 10).

In view of the uncertainty of the orientation of the primary deposition plane for any specific configuration, one may first calculate a maximum arrival rate at a point (x, y, z). This would be the case for a surface oriented normal to the direction of particle flow (i.e., $\cos \alpha_2 = 1.0$). Some typical values of the maximum expected flux ratios, calculated from equation (1), are shown in figure 4 for varying distances ℓ and angles α_1. Notice that even for an α_1 of 85°, the magnitude of the μ/ν ratio is greater than 10^{-5} for distances up to 100, and at $\ell = 100$, the μ/ν ratio for $\alpha_1 = 85^\circ$ is only one order of magnitude less than the value for $\alpha_1 = 0^\circ$. The value of 10^{-5} will be shown later to represent a significant neutral flux. Of course, if there is more than one source of particle flux to a particular surface (i.e., more than one thruster), values of μ from each must be determined and the values summed. The μ/ν values from figure 4 cannot be summed directly unless the source emission rates are all equal. Under the assumptions of free-molecule flow, no interaction between the neutral effluxes from the separate sources would be anticipated.

If, by means of the preceding calculation procedure, the maximum expected arrival rate at any point in question on the spacecraft is clearly too small to be of consequence to the particular spacecraft design, a more accurate calculation of the flux ratio is unnecessary. If, on the other hand, additional calculations are indicated because of the magnitudes being significant, the additional geometric factor $\cos \alpha_2$ for the specific orientation must be calculated for each thruster and applied to the values in figure 4. This will be done for the illustrative problem presented later.

Secondary surfaces. - The values of return flux ratios can be estimated using a coordinate system comparable to figure 3. As shown in figure 5, the secondary surface is arbitrarily placed in the z-y plane and a point of interest is selected at (a', b', c'). The ratio of the arrival rate at (a', b', c'), via (x, y, z), to the source efflux at (a, b, c) is derived through the product of the following readily obtainable ratios

$$\frac{\mu'}{\nu} = \left(\frac{\mu}{\nu}\right)\left(\frac{\mu'}{\nu_o}\right)\left(\frac{\nu_o}{\mu}\right) \tag{2}$$

where

μ' particle flux to surface at (a', b', c')

ν_o flux leaving surface at (x, y, z)

If it is assumed that condensation on the (x, y, z) surface is not occurring, or that equilibrium has been reached, all the flux that arrives there will leave (i.e., $\mu = \nu_0$). In this case, equation (2) becomes

$$\frac{\mu'}{\nu} = \frac{\cos \alpha_1 \cos \alpha_2}{\ell^2} \frac{\cos \alpha_3 \cos \alpha_4}{(\ell')^2} r^2 \tag{3}$$

The factor r^2 appears in equation (3) because the "view" factor for the returning flux ratio μ'/ν_0 must be based on the primary reflecting surface area, but the dimensionless distances ℓ and ℓ' have been defined in terms of the source (thruster) radius. Therefore, r is a radius of an emitting area on the primary surface, nondimensionalized to the thruster radius.

As before, a maximum relative flux ratio from (x, y, z) to (a', b', c') is obtained for an (a', b', c') orientation perpendicular to ℓ' (i.e., when $\cos \alpha_4 = 1.0$). Calculation of the flux ratio μ'/ν at some specific secondary surface location is illustrated by choosing arbitrarily a point located back at the source center ($\ell = \ell'$). Return flux at this location will be representative for surfaces near the thruster plane, but outside a region subject to direct impingement. There will be a maximum back flux at that point for the conditions $\cos \alpha_2 = \cos \alpha_3 = \cos \alpha_4 = 1.0$, so that the return flux ratio is simply

$$\frac{\mu'}{\nu} = \frac{\cos \alpha_1}{\ell^4} r^2 \tag{4}$$

Some representative values of return flux ratios from equation (4) are shown in figure 6 for $r = 1$, that is, for a reflecting area equal to the thruster area. Obviously, the return flux would be greater for larger primary reflecting surfaces.

Equation (4) differs from equation (1) simply by the factor r^2/ℓ^2; however, it is interesting to note that, even for an α_1 of 85^o, the magnitude of the return flux ratio is greater than 10^{-5} for distances up to 10 thruster radii. Significant neutral flux is indicated for this value of 10^{-5} as shown later. Again, if there is more than one thruster or more than one reflecting surface (or a larger reflecting surface) that can contribute to return flux, the values of μ' must be determined for each and added to obtain the total, true returning arrival rate. If this estimated maximum appears significant to the particular application, more refined calculations are indicated.

Desorption Rates

The desorption rate of particles from a surface, assuming desorption is first order with respect to surface coverage, is described by the relation (ref. 11)

$$\nu_d = \frac{\sigma}{\tau_o} \exp\left(-\frac{E_{des}}{kT_s}\right) \tag{5}$$

where

ν_d desorption rate

σ surface concentration

τ_o constant, 10^{-13} sec

E_{des} desorption energy

k Boltzmann constant

T_s surface temperature

Desorption rates for fractional monolayer coverages are discussed in reference 12. In the present application, desorption rates for greater than monolayer coverage are of primary concern, that is, for desorption of propellant from its own solid surface. The value of σ_m (surface concentration for a monolayer coverage) for a material depends on the crystal face involved (ref. 13). For a polycrystalline surface, the 2/3 root of the number density of the solid can be used as a good approximation to the surface density

$$\sigma_m \cong \left(\frac{\rho}{M}\right)^{2/3} \tag{6}$$

where

ρ density of solid

M weight of surface atom

Equation (5) thus reduces to

$$\nu_d = \frac{1}{\tau_o}\left(\frac{\rho}{M}\right)^{2/3} \exp\left(-\frac{E_{des}}{kT_s}\right) \tag{7}$$

Values of ρ/M and E_{des} (heat of sublimation in these cases (ref. 14)) for a number of materials are shown in table I and desorption rates calculated according to equation (7) are shown in figure 7. Data for a number of materials from table I are shown therein also. Values of desorption rate of a material from figure 7 will be used in the illustrative example presented later to compare with calculated arrival rates to determine whether condensation conditions exist at a particular surface.

DISCUSSION AND ILLUSTRATIVE PROBLEMS

The first assumption made here is that, as portrayed in figure 1, the spacecraft configuration will at some time require the location of a surface downstream of the plane of the thruster exhaust (otherwise no problem exists). The objective is to determine if the rate of propellant impingement onto primary surfaces is high enough to create any problems on those surfaces, or on secondary surfaces which may be receiving reflected propellant.

The neutral atom emission rate for an electric thruster is readily calculated from

$$n_a = \frac{J}{q}\left(\frac{1-\eta}{\eta}\right) = \frac{I}{A_t q}\left(\frac{1-\eta}{\eta}\right) \tag{8}$$

where

J ion beam current density

q electron charge

η propellant utilization efficiency, fraction of total propellant flow which is ionized

I ion beam current

A_t thruster area

Thus, for example, a bombardment thruster with a beam current of 30 amperes per square meter and a utilization efficiency of 90 percent would have a neutral atom emission rate of $n_a = 2.1\times10^{15}$ atoms per square centimeter per second.

It can be noted, using figure 4, then, that arrival rates at $\ell = 10$, for example, may be as high as 2.1×10^{12} to 2.1×10^{13} atoms per square centimeter per second. With mercury as the propellant, this arrival flux represents possible condensation rates (depending on component temperatures) of 0.0017 to 0.017 monolayer per second, or from about 150 to 1500 monolayers per day. Not only is this situation a possibly troublesome one, but also, with any sizable surface area so exposed to this neutral flux, the return flux to areas behind the thruster plane could also be of concern. From figure 6, note that for

the same distance, $\ell = 10$, the return flux ratio is 10^{-5} to 10^{-4}. Thus, even from a reflecting area only as large as the thruster area (i.e., $r = 1$), the possible return flux rates from this distance would be equivalent to from 1.5 to 15 monolayers per day. From larger reflecting areas, and with more than one thruster operating, this return flux would be proportionately greater. More detailed calculations would be required depending on the spacecraft design and mission profile.

Spacecraft Configurations

Two solar-electric spacecraft configurations, proposed for Jupiter flyby probes (refs. 7 and 8), have been used to illustrate more specific calculations of the magnitudes of direct propellant flux to primary surfaces and return propellant flux to secondary surfaces. These spacecraft designs were selected for comparison because they differ in their orientation of the solar panel array with respect to the thruster locations. They will, therefore, permit some comparison of the effect of solar-array - thruster orientation on the possible propellant flux problems.

The two configurations are shown schematically in figures 8 and 9. Hereinafter, for convenience, they are referred to as JFB-1 and JFB-2, respectively. The JFB-1 spacecraft (fig. 8(a)) has solar panels that extend to about a 15-meter radius and which can pivot about the z-axis. The panels can therefore extend out downstream of the thruster plane at various rotation angles (fig. 8(b)). According to reference 7, the craft would be used for a direct trajectory flyby and would have a total thrusting time of 470 days. Thrust would be obtained from four 2.5-kilowatt mercury bombardment thrusters.

For the JFB-1 spacecraft, the mission profile discussed in reference 7 yields the time variation of panel angle, range, and thruster propellant flow rate pertinent to this discussion shown in figure 10. The total neutral mercury arrival rate at any location on the solar panels for any time during the mission can be calculated through use of the curves of figure 10 and equation (1).

The JFB-2 spacecraft (fig. 9) was suggested in reference 8 in an approach aimed at simplification of electric spacecraft design. The design resulting from this study had a fixed orientation of the thrusters relative to the solar panels and thus provided an interesting and contrasting configuration for the present flux problem discussion. The dimensions used herein for calculation purposes are estimated values, based on the required solar panel area and the general orientation, as indicated in figure 9. Only the portions of the solar panels which extend beyond the thruster exit plane are subject to direct impingement of neutral flux from the thrusters. Figure 9(b) shows the details of the configuration for this portion of the spacecraft. For purposes of calculation, the thrusters and mission profile have been assumed to be identical in every respect to

those used for the JFB-1 design, except for their relative locations, as shown in figure 9(b).

Direct Flux to Solar Panels

Calculated values of the flux ratio μ/ν (see appendix B) from four thrusters located at (x, y, z) values of (0.61, ±0.61, ±0.61 m) are shown in figure 11 for the JFB-1 spacecraft. Various combinations of thruster locations were investigated. The one illustrated here was selected as typical, there being no significant differences in conclusions arrived at between any of the locations chosen. Results for three panel angles relative to the y-z plane are given. The flux is shown along the diagonal axis and along the upper and lower edges of the panel (see fig. 8). Because of the spacecraft configuration and Sun orientation, at panel angles between 45° and 135°, the flux to the Sun side of the panels comes from only two thrusters. At these angles, neutral efflux from the other two thrusters impinges on the back side of the panel. By virtue of symmetry, arrival rates on the Sun side at a given angle β are identical to those on the back side at an angle $180^{\circ} - \beta$.

For propellant flow rates encountered during the early stages of the mission, flux rates of the order of 100 to 200 monolayers per day may strike the portions of the solar array closest to the thrusters. At the extremities of the configuration, the flux rates are considerably lower, around 1/2 to 1 monolayers per day.

For the JFB-2 configuration, because of the fixed relation of solar panel to thruster location, the ratio of neutral flux arriving at any point on the solar panel to thruster neutral efflux, remains fixed throughout the mission. The actual magnitude of flux, of course, will decrease as propellant flow rate decreases during the mission. The direct flux ratios and flux rates at the higher propellant flow rates are shown in figure 12. The total flux rates, up to 500 monolayers per day on some portions and over 30 monolayers per day over most of the array, are an order of magnitude higher than for the JFB-1 design because the array is closer to the thruster exhaust in this design.

Return Flux to Spacecraft

Return flux to points in a plane at $x = 0$ have been calculated for both configurations (see appendix B). The contribution from all the solar panel area has been accounted for. These calculated rates are shown in figures 13 and 14 for the JFB-1 and JFB-2 spacecraft, respectively.

Return flux ratios for the JFB-1 configuration reach values of about 3.3×10^{-5}, equivalent to a neutral impingement rate of about 3.8 monolayers per day, at some

locations in the $x = 0$ plane. For the JFB-2 design, the return fluxes ranged beyond 25 monolayers per day at some locations in the $x = 0$ plane. Again, this latter configuration has much higher flux values because the array is close to the plane in question, and also because direct flux values on the array are higher.

As noted in the previous figures and discussion, the impingement rates are strongly dependent on the distance of surfaces from the thrusters. But the point to be emphasized is simply that, even outside the cone angle of the main ion beam, considerable propellant atom flow can arrive at structural surfaces which lie downstream of the thruster exit plane. Whether the magnitude of this arrival rate of propellant is sufficient to cause any operational problems for that surface is another question. However, one can calculate whether or not the propellant may condense and build up a covering layer on the panels. To estimate this situation, it is necessary to consider the several factors controlling the solar panel temperature; that is, the complete mission profile must be considered.

Condensation Possibilities

The equilibrium temperature of a panel at any location in space is calculated from a radiation heat balance

$$Q_E \frac{\alpha_f \cos \gamma}{R^2} = \sigma(\epsilon_f + \epsilon_b)T_p^4 \tag{9}$$

or

$$T_p = \left[\frac{Q_E \cos \gamma}{R^2 \sigma}\left(\frac{\alpha_f}{\epsilon_f + \epsilon_b}\right)\right]^{1/4} \tag{10}$$

where

Q_E solar constant

α_f solar absorptance of panel surface facing Sun

γ angle between surface normal and Sun line

R distance from Sun

σ Stefan-Boltzmann constant

ϵ_f, ϵ_b thermal emittance of front and back surfaces of panel, respectively

The values of ϵ_f and ϵ_b depend on the nature of the surface and whether or not it has condensate on it. (Recent experimental investigations have been undertaken at the

Lewis Research Center to determine values for α and ϵ for thin-film solar cells (refs. 15 and 16).) The equilibrium temperature T_p from equation (10) is plotted in figure 15 for a range of $\alpha_f/(\epsilon_f + \epsilon_b)$ values, and for $\gamma = 0$, that is, a surface normal to the Sun line. If the thermal properties of the surface do not change, the surface temperature falls inversely with the square root of the range. The solar panel temperature, necessary to estimate possible desorption rates from the panel by equation (5) or (7), can be obtained from figure 15. However, the α/ϵ ratio to use for determining the temperature will depend on whether condensation can occur, since, in general, the condensate layer would be expected to have different thermal properties than the panel itself.

Some representative values of α and ϵ for clean surfaced solar cells (refs. 15 and 16) and for a mercury surface (refs. 4 and 17) are shown in table II, along with the resulting values of $\alpha_f/(\epsilon_f + \epsilon_b)$ for the various possible combinations of surfaces. Higher values of $\alpha_f/(\epsilon_f + \epsilon_b)$ result in higher equilibrium temperatures (fig. 15) for any given heat input rate. Those combinations which have a higher value of $\alpha_f/(\epsilon_f + \epsilon_b)$ than that of the clean panels will, then, be self-cleaning in a sense; that is, any tendency of a deposit to form on surfaces in a way which would raise the $\alpha_f/(\epsilon_f + \epsilon_b)$ ratio would tend to raise the panel temperature. The resulting increased desorption rate would then tend to clean the panel of adsorbate. Such is the case in this illustration for mercury condensation on the back surface of the solar panel only, or on both front and back surfaces simultaneously. However, an essentially indeterminate situation may result for the case of mercury condensation on the front surface only. Because the resulting ratio of $\alpha_f/(\epsilon_f + \epsilon_b)$ is lower for this condition than for a clean panel, the panel temperature for a front-surface-coated panel would be lower than for a clean panel. One can see, therefore, that there may be conditions where, if a panel were covered with condensate, condensation could continue, whereas if the panel were clean its higher temperature might prevent condensation. Therefore, it is clear that the actual equilibrium conditions of the surface may depend on its previous history.

From a knowledge of the mercury arrival rate at a point on the panel and the desorption rate curve for mercury (one condition is illustrated in fig. 7), one can determine an equilibrium temperature (i.e., a temperature where the adsorption rate and desorption rate are equal). The equilibrium temperature-arrival rate relation for mercury is plotted in figure 16 for a range of temperatures of interest to this discussion.

The equilibrium temperature levels calculated for the direct arrival rates at two locations on the panels are shown in figure 17. The dashed lines are lines of constant $\alpha_f/(\epsilon_f + \epsilon_b)$ for clean solar cells (upper band) and mercury-coated cells (lower line). The clean panel temperature level is shown by a band reflecting the spread in experimentally determined optical properties (table II). Whether condensation will occur on the panel depends on the applicable value of $\alpha_f/(\epsilon_f + \epsilon_b)$. If the actual panel temperature is below the calculated temperature representing the equilibrium arrival rate, a condensate layer can build up at that location on the panel.

The results shown in figure 17 should be interpreted in the following manner. If the panel is clean (i.e., no mercury on it), condensation should not occur on the near portions of the panel until the spacecraft is at about 2.5 to 2.7 astronomical units. Portions of the panel farther from the thrusters, of course, will not be cool enough to condense propellant until later in the mission. For example, the near edge of the wide panel section would not reach condensation conditions until 2.8 to 3.2 astronomical units, or very near the end of the thrusting period of this mission.

For the JFB-2 spacecraft, as noted in figure 17(b), the higher fluxes result in condensation conditions being reached earlier in the assumed flight schedule at around 2.25 to 2.5 astronomical units. Even the farther areas of the solar panel would encounter condensing conditions by about 2.6 to 2.8 astronomical units.

Actually, at about 1.9 to 2 astronomical units for JFB-1, and 1.7 to 1.9 astronomical units for JFB-2, the flux levels and possible panel temperatures approach the condition of indeterminacy mentioned previously. Without a condensate layer present, the panel temperature would be expected to remain above the condensation level. However, if the panel temperature should be somehow temporarily lowered below the condensation temperature, due to misorientation for example (and permitting mercury to condense on the Sun side of the panel), the resulting value of the parameter $\alpha_f/(\epsilon_f + \epsilon_b)$ would be such as to keep the panel temperature below the condensation level and the condensate layer would continue to grow. Thus, the importance of panel temperature history during the mission is evident.

Figure 18 shows a situation similar to that described in figure 17 for return fluxes arriving at an imaginary plane (x = 0) upstream of the thrusters. Figure 18(a) for the JFB-1 design shows that condensation could occur at some point on the panel at temperatures below the values indicated by peak flux curve. It can be seen further from the lower curve that condensation could occur somewhere in the region (y, z) = (6.1, 6.1) meters at temperatures of 165 to 185 K. The temperature levels shown by the α/ϵ lines are for an assumed surface which sees the Sun directly. Of course, any surface which is not so oriented, or receives no other source of heat, could easily be cool enough to have mercury condense on it.

The JFB-2 configuration, with higher return flux values, also has a higher temperature level below which condensation could occur, about 180 to 200 K. Most of the area within a (y, z) range of (3, 3) meters has flux levels greater than 0.1 times the peak flux.

CONCLUDING REMARKS

Consideration of the neutral atom efflux to be expected from the thrusters on electric spacecraft has led to the following general conclusions:

1. Estimates of probable maximum neutral propellant arrival rates on surfaces of an electric spacecraft can be easily made using simplified molecular flow relations. The magnitude of these probable maximum rates can be reviewed in consideration with the planned mission profile to determine whether more detailed calculations are required.

2. For two missions studied, efflux rates at neutral particles were high enough and interplanetary flight times long enough that considerable total propellant could impinge on nearby spacecraft surfaces located downstream of the thruster exhaust plane.

3. Surfaces not in the line of sight of initial propellant atom trajectories may still receive impingement through reflection or reevaporation from surfaces in the direct line of sight of the thruster exhaust.

4. Mercury flux rates onto the solar panels of two proposed JFB spacecraft are such that propellant condensation on the portion of the panels close to the thruster could occur in the latter stages of the mission. Specifically, this situation occurs when the spacecraft is at about 1.7 to 2.0 astronomical units. In time, the portions over which condensation can occur then extend outward away from the thrusters, up to and including the most remote portions of the solar cell panels.

5. The example problems illustrated the importance of the solar panel temperature history throughout the mission. It was shown that an unplanned premature cooling of the panel could upset the thermal equilibrium of the situation sufficiently to cause unexpected condensation to occur. The condensate might reevaporate or condensation might then continue depending on which surfaces were affected.

Lewis Research Center,
National Aeronautics and Space Administration,
Cleveland, Ohio, September 9, 1969,
120-26.

APPENDIX A

SYMBOLS

[All equations in the text require linear dimension variables to be used as dimensionless ratios to the thruster radius. Otherwise, any consistent set of units may be used.]

A_p area of primary surface

A_t thruster area

a x-spacing of thruster (fig. 3)

a' x-coordinate point on secondary surface (fig. 5)

b y-spacing of thruster (fig. 3)

b' y-coordinate point on secondary surface (fig. 5)

c z-spacing of thruster (fig. 3)

c' z-coordinate point on secondary surface (fig. 5)

E_{des} desorption energy

I current

J current density

k Boltzmann constant

ℓ distance from thruster to point on primary surface (figs. 3 and 5)

ℓ' distance from point on primary surface to point on secondary surface (fig. 5)

M weight of substrate atom

n_a neutral atom emission rate

Q_E solar constant at 1.0 AU

q electron charge

R range; distance from Sun in AU

r radius of emitting area on primary surface

S sticking coefficient

T_p equilibrium temperature of solar panel, K

T_s surface temperature, K

t time, sec

x general coordinate dimension (fig. 3 or 5)

x_i coordinate on JFB-2 panel (fig. 9(b))

y general coordinate (fig. 3 or 5)

y_i coordinate on JFB-2 panel (fig. 9(b))

y_o coordinate on JFB-1 panel at $\beta = 0$ (eqs. (B1) and (B2))

y_r coordinate on plane at x = 0 (fig. 9(b), eqs. (B2) and (B4))

z general coordinate (fig. 3 or 5)

z_o coordinate on JFB-1 panel at $\beta = 0$ (eqs. (B1) and (B2))

z_r coordinate on plane at x = 0 (fig. 9(b), eqs. (B2) and (B4))

α_f absorptance of Sun side of solar array

α_1 angle between thruster plane normal and line to point on primary surface (fig. 3)

α_2 angle between primary surface normal and line from thruster (fig. 3)

α_3 angle between primary surface normal and line to point on secondary surface (fig. 5)

α_4 angle between secondary surface normal and line to point on primary surface (fig. 5)

β angle of rotation of solar array of JFB-1 spacecraft

γ angle between surface normal and Sun line

ϵ_b thermal emittance of back surface of solar panel

ϵ_f thermal emittance of front (Sun side) surface of solar panel

η propellant utilization efficiency

μ arrival rate

μ' arrival rate at secondary surface

ν leaving rate

ν_d desorption rate

ν_o leaving rate from primary surface

ρ density of solid

σ surface concentration

σ_m surface concentration of a complete monolayer

τ_o constant in desorption equation (eq. (5), sec

APPENDIX B

DETAILS OF RELATIONS FOR FLUX CALCULATIONS

Direct flux values to the primary surface of the JFB-1 design were calculated from the relation, for a single thruster,

$$\frac{\mu(y_o, z_o, \beta)}{\nu} = \frac{(y_o \sin \beta - a)(a \cos \beta - b \sin \beta)}{\left[(y_o \sin \beta - a)^2 + (y_o \cos \beta - b)^2 + (z_o - c)^2\right]^2} \tag{B1}$$

where

y_o, z_o coordinates of a point on the solar panel at $\beta = 0$

β rotation angle of solar panel

a, b, c x, y, z locations, respectively, of thruster (four thrusters were accounted for: (a, b, c) = (2, ±2, ±2))

μ neutral atom arrival rate at a surface

ν neutral atom emission rate of source

The return flux values to the plane at $x = 0$ were determined from the relation

$$\frac{\mu(0, y_r, z_r)}{\nu} = \int_{A_p} \frac{y_o \sin \beta (y_r \sin \beta)}{\left[(y_o \sin \beta)^2 + (y_o \cos \beta - y_r)^2 + (z_o - c)^2\right]^2} \left[\frac{\mu(y_o, z_o, \beta)}{\nu}\right] dA_p \tag{B2}$$

where

y_r, z_r coordinates of a point on the imaginary panel at $x = 0$

dAp differential area of solar panel

Direct flux values to the primary surface of the JFB-2 design were calculated from the relation, for a single thruster,

$$\frac{\mu(x_i, y_i)}{\nu} = \frac{y_i(c)}{\left(x_i^2 + y_i^2 + z_i^2\right)^2} \tag{B3}$$

where x_i, y_i are coordinates of a point on the solar panel (primary surface). Four thrusters were accounted for at $a = 2$, $b = 0$, and $c = 2$, 4, 6, and 8.

The return flux values to the plane at $x = 0$ were determined from the relation

$$\frac{\mu(0, y_r, z_r)}{\nu} = \int_{A_p} \frac{z_r x_i}{\left[x_i^2 + (y_i - y_r)^2 + z_r^2\right]^2} \frac{\mu(x_i y_i)}{\nu} \, dA_p \tag{B4}$$

The integration of equations (B2) and (B4) were done numerically. The contributions of the two sections of the solar panels were accounted for by integrating equations (B2) and (B4) for both positive and negative values of y_r.

REFERENCES

1. Nöller, H. G.: Approximate Calculation of Expansion of Gas from Nozzles into High Vacuum. J. Vacuum Sci. Tech., vol. 3, no. 4, July/Aug. 1966, pp. 202-207.

2. Grier, Norman T.: Back Flow from Jet Plumes into Vacuum. NASA TN D-4978, 1969.

3. Staggs, John F.; Gula, William P.; and Kerslake, William R.: Distribution of Neutral Atoms and Charge-Exchange Ions Downstream of an Ion Thruster. J. Spacecraft Rockets, vol. 5, no. 2, Feb. 1968, pp. 159-164.

4. Hall, David F.; Newman, Brian E.; and Womack, James R.: Electrostatic Rocket Exhaust Effects on Solar-Electric Spacecraft Subsystems. Paper 69-271, AIAA. Mar. 1969.

5. Kerslake, William R.; Byers, David C.; and Staggs, John F.: SERT II Experimental Thruster System. Paper 67-700, AIAA, Sept. 1967.

6. Kerslake, William R.: Charge-Exchange Effects on the Accelerator Impingement of an Electron-Bombardment Ion Rocket. NASA TN D-1657, 1963.

7. Barber, T. et al.: 1975 Jupiter Flyby Mission Using a Solar Electric Spacecraft. Rep. ASD 760-18, Jet Propulsion Lab., California Inst. Tech., Mar. 1, 1968.

8. Barber, T. A.; and Meissinger, H. F.: Simplification of Solar-Electric Propulsion Missions by a New Staging Concept. Paper 69-251, AIAA, Mar. 1969.

9. Patterson, G. N.: A State-of-the-Art Survey of Some Aspects of the Mechanics of Rarefied Gases and Plasmas. Toronto Univ. (ARL-64-60, DDC No. AD-600873), Apr. 1964.

10. Reynolds, Thaine W.; and Richley, Edward A.: Free-Molecule Flow and Surface Diffusion through Slots and Tubes. A Summary. NASA TR R-255, 1967.

11. DeBoer, J. H.: Adsorption Phenomena. Advances in Catalysis. Vol. 8. W. G. Frankenberg, V. I. Komerewsky, and C. K. Rideal, eds., Academic Press, 1956, pp. 17-161.

12. Reynolds, Thaine W.: Adsorption-Desorption Behavior of Homogeneous and Heterogeneous Metal Surfaces. NASA TN D-4789, 1968.

13. Bacigalupi, Robert J.: Surface Topography of Single Crystals of Face-Centered-Cubic, Body-Centered-Cubic, Sodium Chloride, Diamond, and Zinc-Blende Structures. NASA TN D-2275, 1964.

14. Honig, R. E.: Vapor Pressure Data for the Solid and Liquid Elements. RCA Rev., vol. 23, no. 4, Dec. 1962, pp. 567-586.

15. Liebert, Curt H.; and Hibbard, Robert R.: Theoretical Temperatures of Thin-Film Solar Cells in Earth Orbit. NASA TN D-4331, 1968.

16. Jack, John R.; and Spisz, Ernie W.: Thermal Radiative and Electrical Properties of a Cadmium Sulfide Solar Cell at Low Solar Intensities and Temperatures. NASA TN D-4818, 1968.

17. Parker, W. J.; and Abbott, G. L.: Theoretical and Experimental Studies of the Total Emittance of Metals. Symposium on Thermal Radiation of Solids. S. Katzoff, ed. NASA SP-55, 1965, pp. 11-28.

TABLE I. - PROPERTIES OF VARIOUS MATERIALS

Material	Density to mass ratio, ρ/M, g-mol/cc	Sublimation energy, E_{des}, eV	Monolayer surface concentration, σ_m, atoms/cm^2
Aluminum	0.0997	3.36	1.54×10^{15}
Cesium	.0141	.81	.422
Lithium	.0770	1.65	1.30
Magnesium	.0714	1.52	1.24
Mercury	.0701	.63	1.22
Molybdenum	.1060	6.87	1.61
Nickel	.1510	4.43	2.04
Silver	.0974	2.96	1.52
Sodium	.0422	1.13	.86
Tantalum	.0893	8.10	1.43
Tungsten	.1040	8.75	1.58
Uranium	.0795	5.07	1.33

TABLE II. - OPTICAL PROPERTIES USED FOR CALCULATIONS

Mercury on solar panels	Total hemispherical emittance		Solar absorptance, α_f	Absorptance-emittance ratio, $\frac{\alpha_f}{\epsilon_f + \epsilon_b}$
	Sun side, ϵ_f	Back side, ϵ_b		
None	0.89 to 0.93	0.93 to 0.96	0.72 to 0.86	0.38 to 0.47
Front surface	0.10	.93 to 0.96	0.22	0.21
Back surface	.89 to 0.93	0.10	.72 to 0.86	.82
Both surfaces	0.10	.10	0.22	1.1

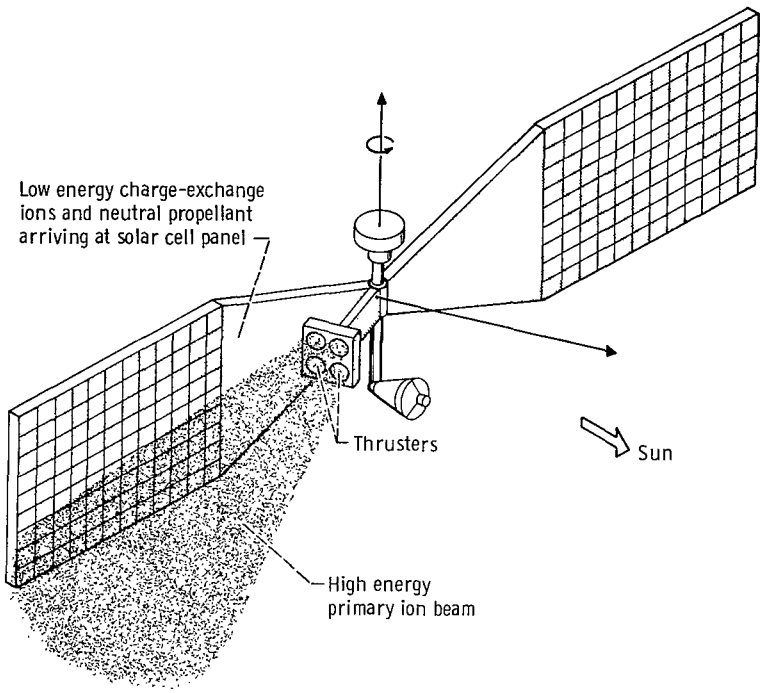

CD-10576-28

Figure 1. - Solar-electric spacecraft.

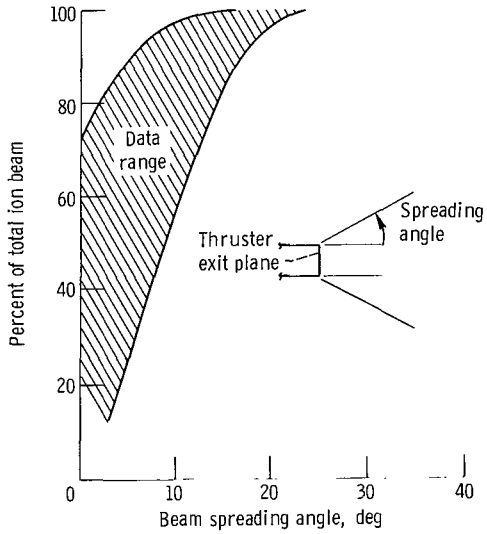

Figure 2. - Summary of mercury ion beam profile surveys. Data range covers several thruster sizes and operating conditions.

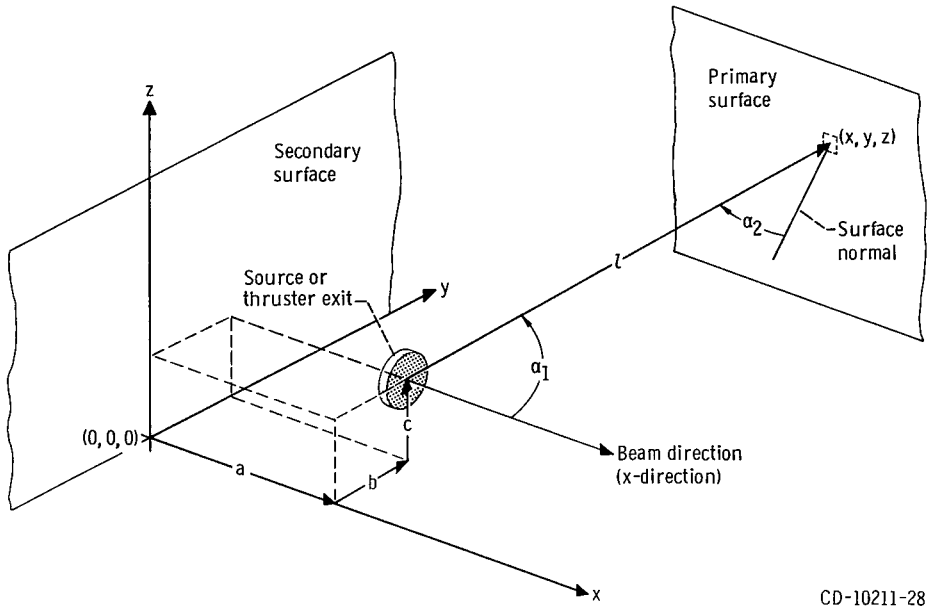

Figure 3. - Coordinate system schematic drawing with direct flux to surface.

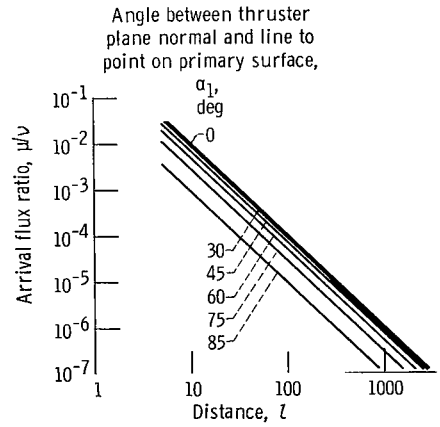

Figure 4. - Maximum expected arrival rate on surface downstream of source.

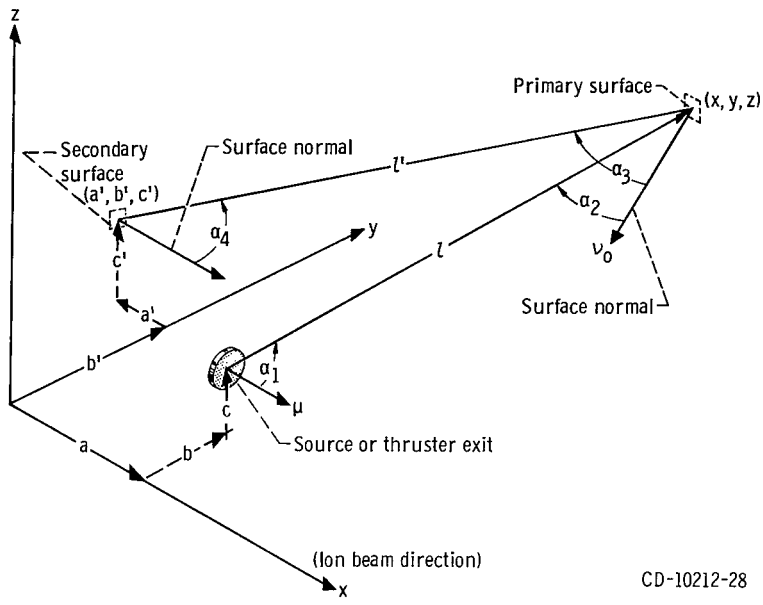

Figure 5. - Coordination system schematic diagram with return flux.

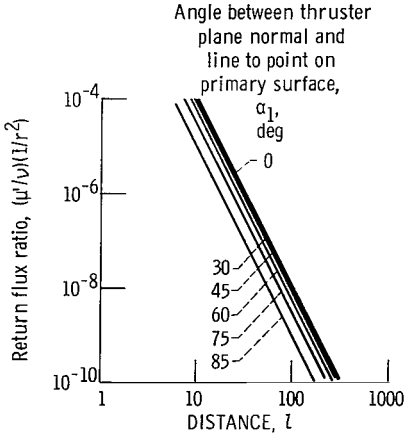

Figure 6. - Maximum expected return rates to surfaces near thruster exit plane.

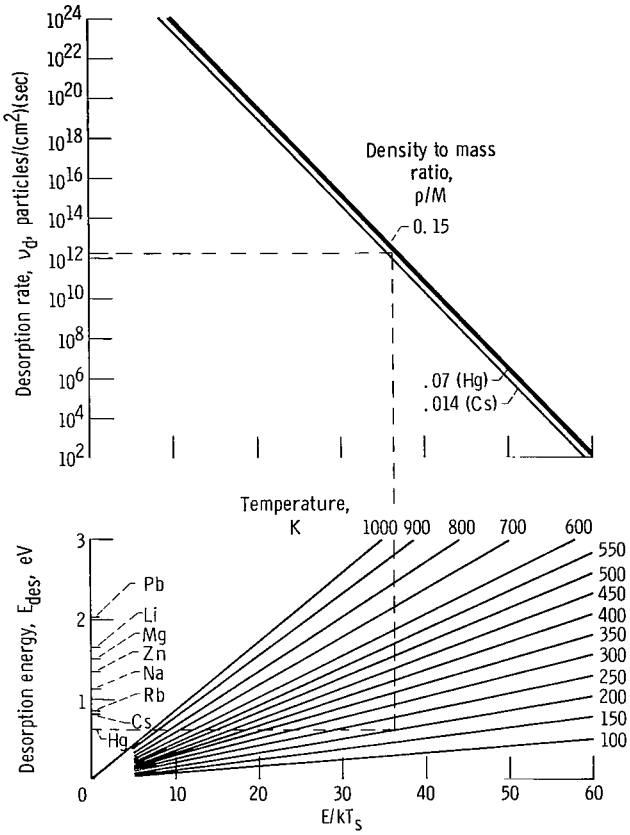

Figure 7. - Desorption rate from monolayer or more concentration as function of temperature, energy, and surface density.

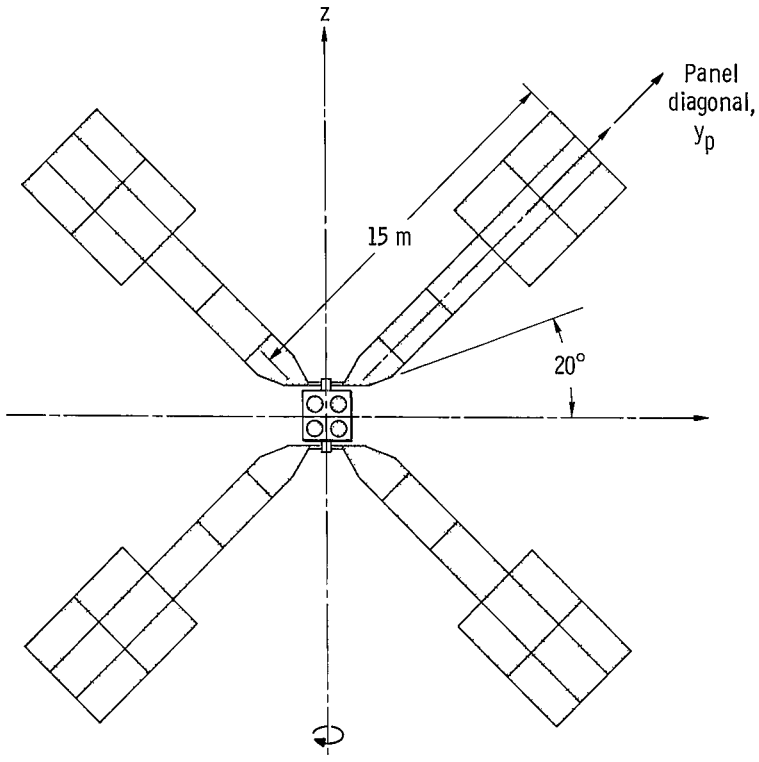

(a) View facing solar panel array. Array rotates about z-axis.

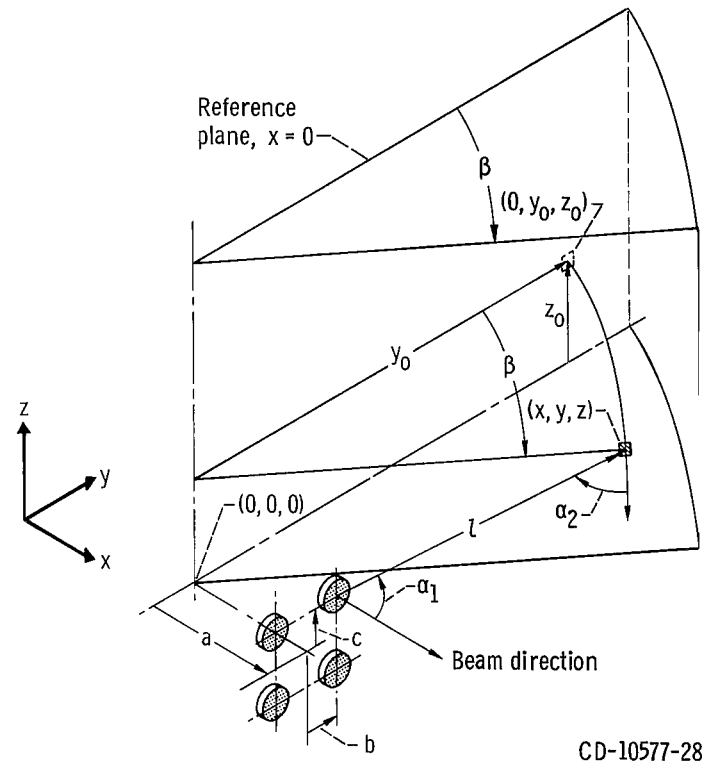

(b) Coordinate system.

Figure 8. - JFB-1 spacecraft schematic drawing.

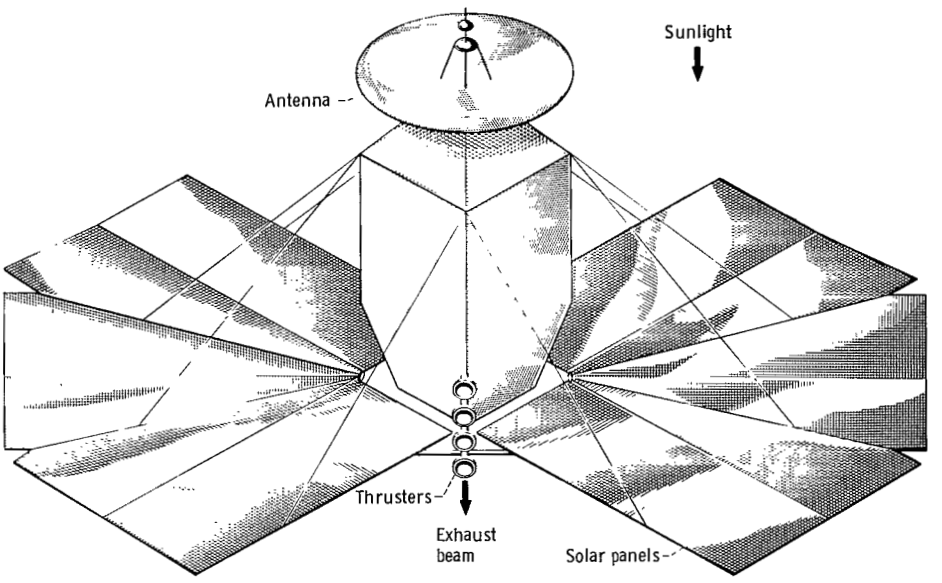

(a) Overall view.

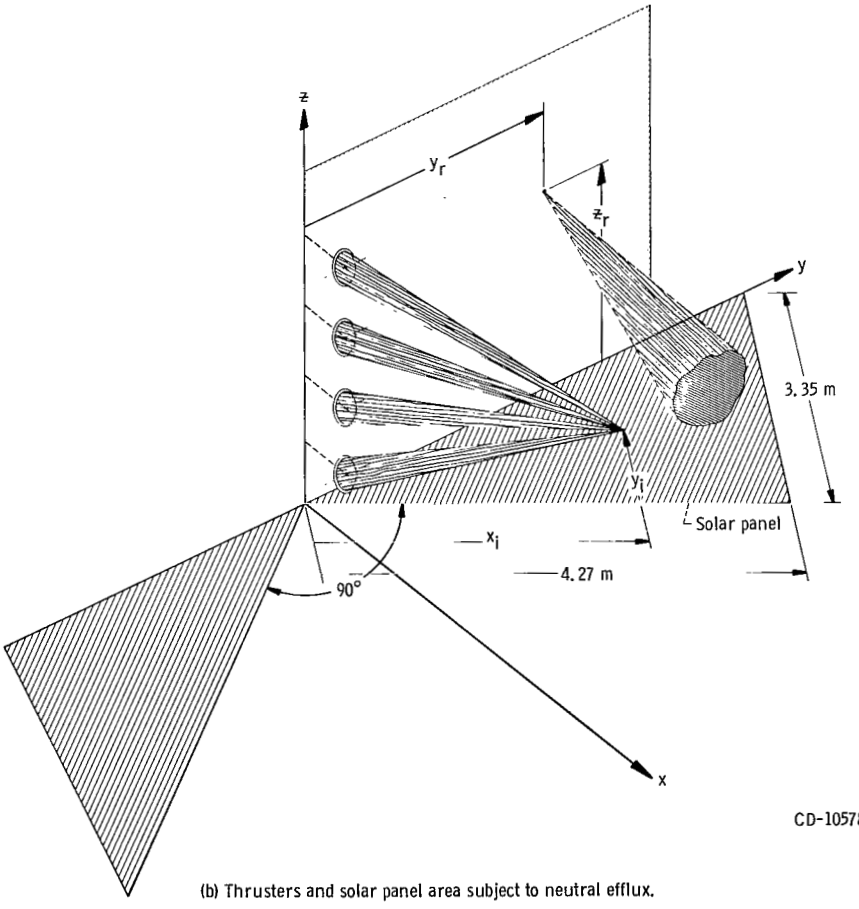

(b) Thrusters and solar panel area subject to neutral efflux.

Figure 9. - JFB-2 spacecraft schematic diagram.

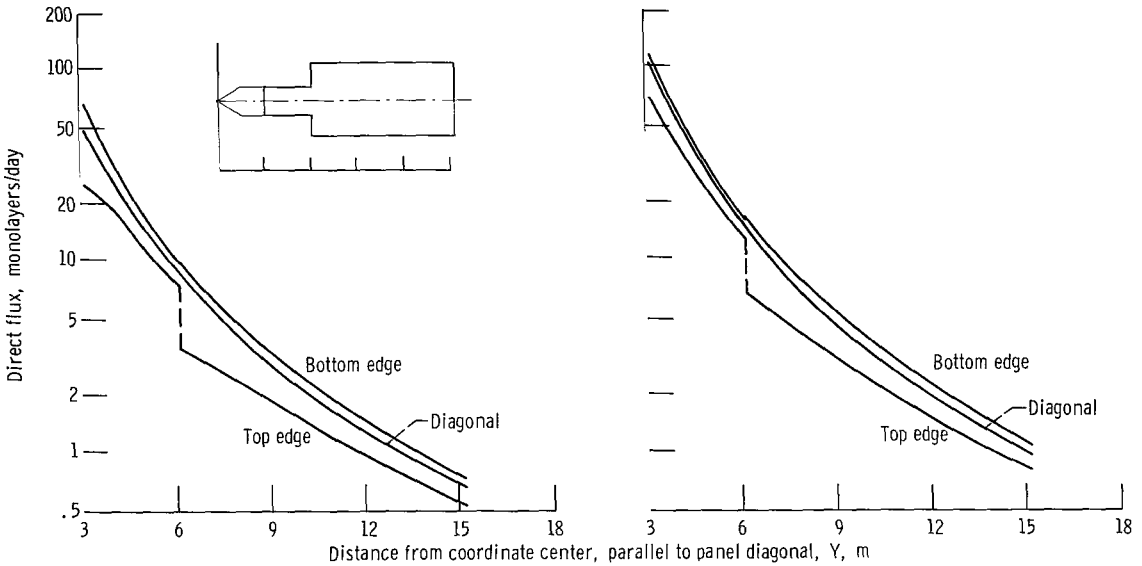

(a) Panel angle, 30°.

(b) Panel angle, 60°.

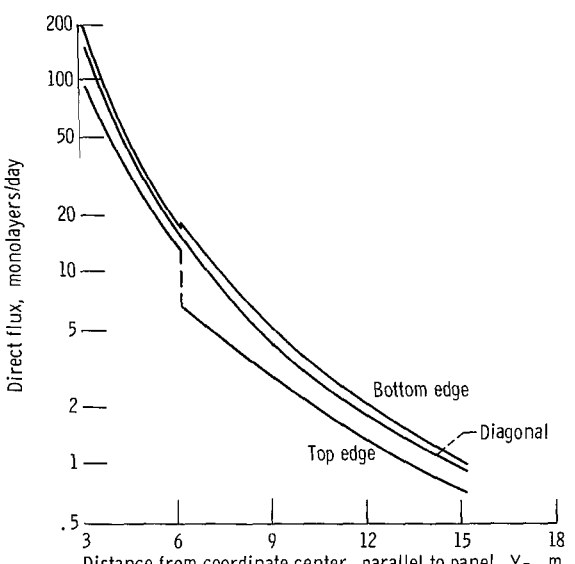

(c) Panel angle, 90°.

Figure 11. - Neutral mercury flux onto JFB-1 solar panels.

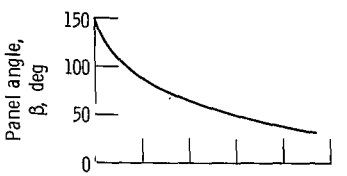

(a) Orientation of panel.

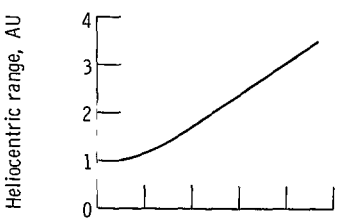

(b) Range of spacecraft.

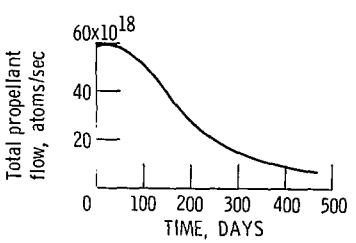

(c) Variation of total propellant flow rate.

Figure 10. - Mission profile variables.

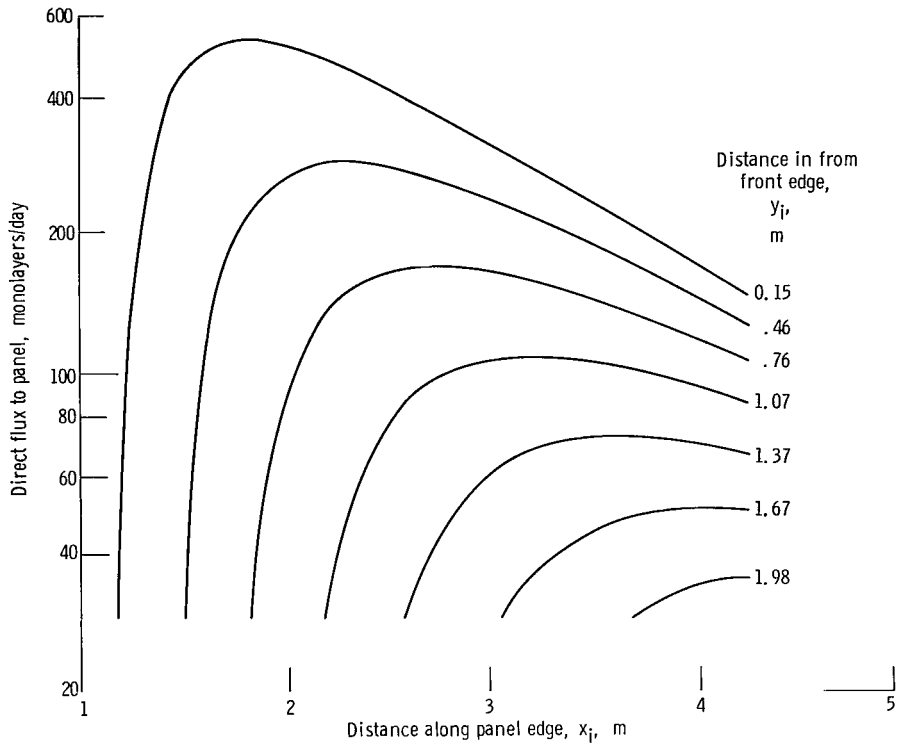

Figure 12. - Neutral mercury flux onto JFB-2 solar panels.

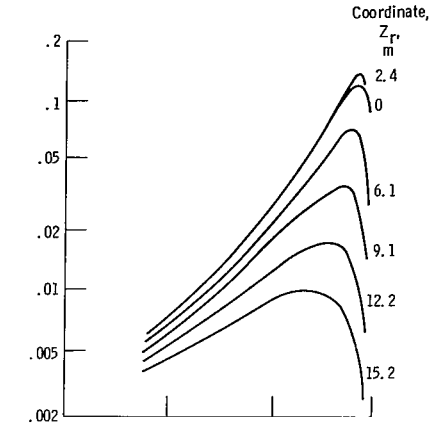

(a) Panel angle, 30° (zero return flux to positive side).

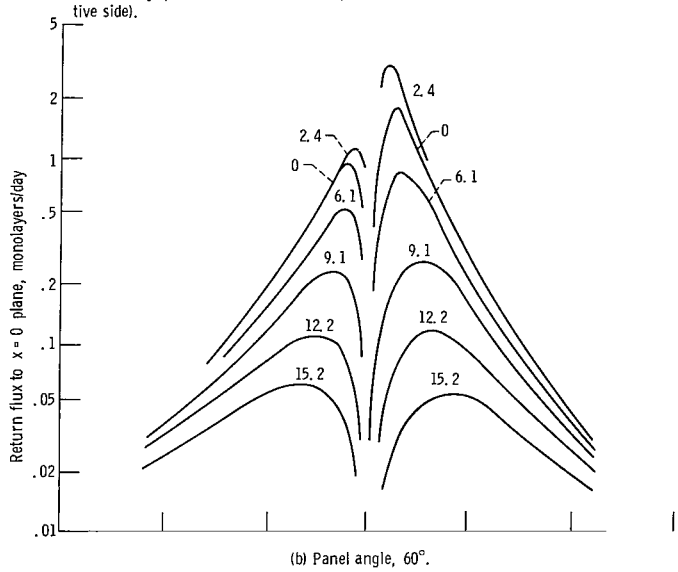

(b) Panel angle, 60°.

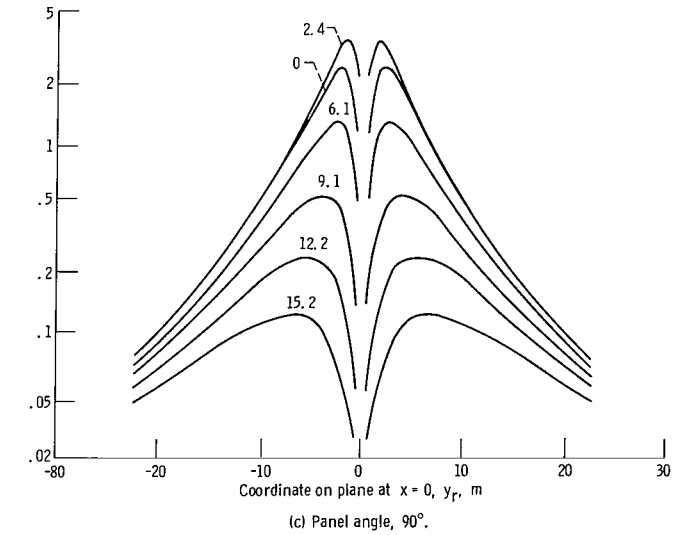

(c) Panel angle, 90°.

Figure 13. - JFB-1 spacecraft neutral mercury return flux at x = 0 plane (see fig. 8(b)).

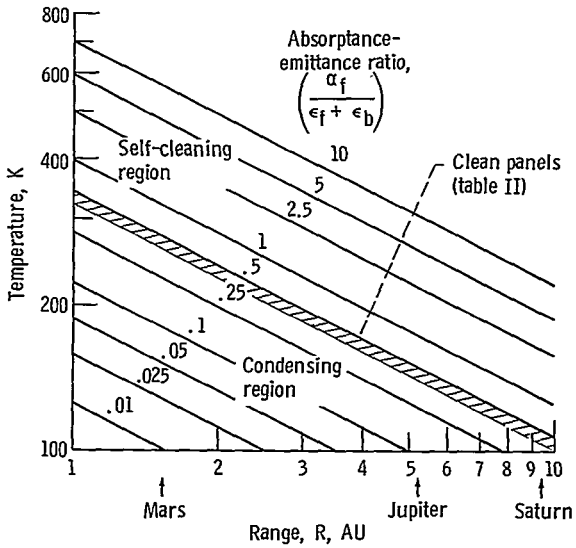

Figure 15. - Variation of equilibrium panel temperature with distance from Sun for varying surface thermal properties.

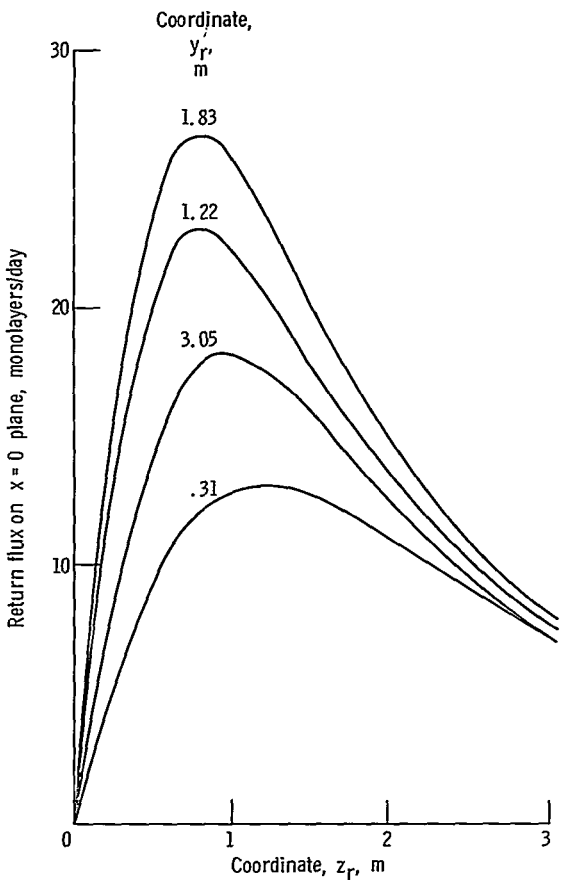

Figure 14. - JFB-2 spacecraft neutral mercury return flux at x = 0 plane (see fig. 9(b)).

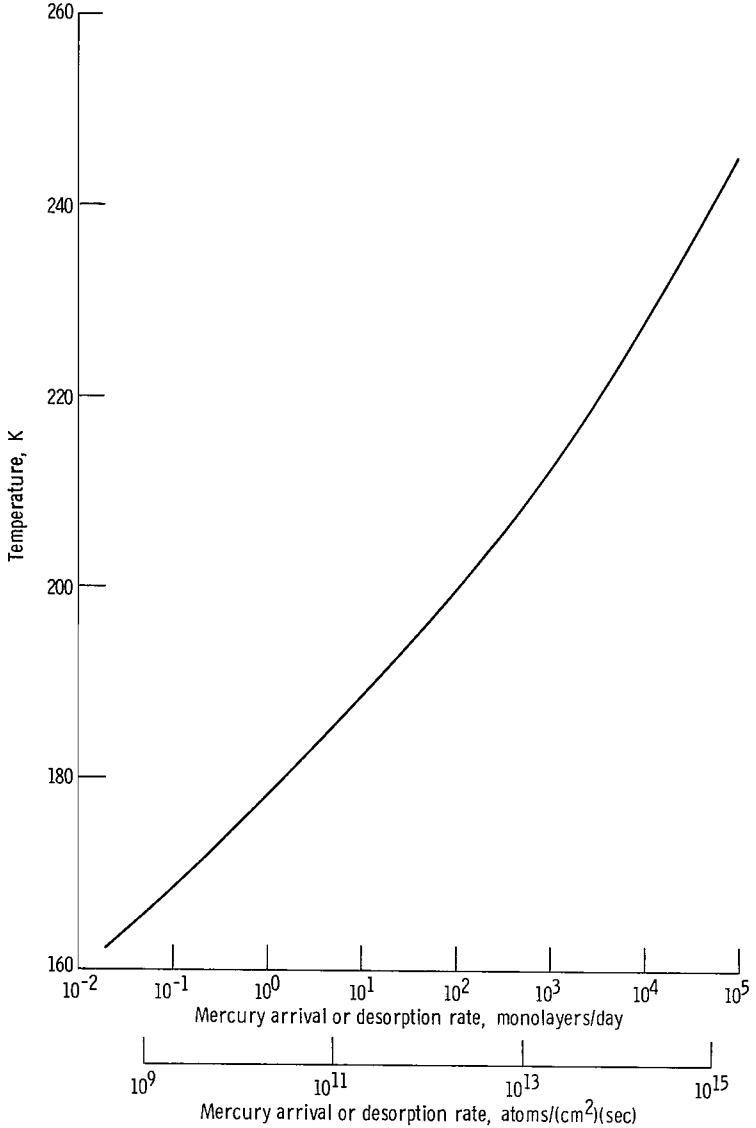

Figure 16. - Variation of equilibrium arrival rate (or desorption rate) of mercury with temperature.

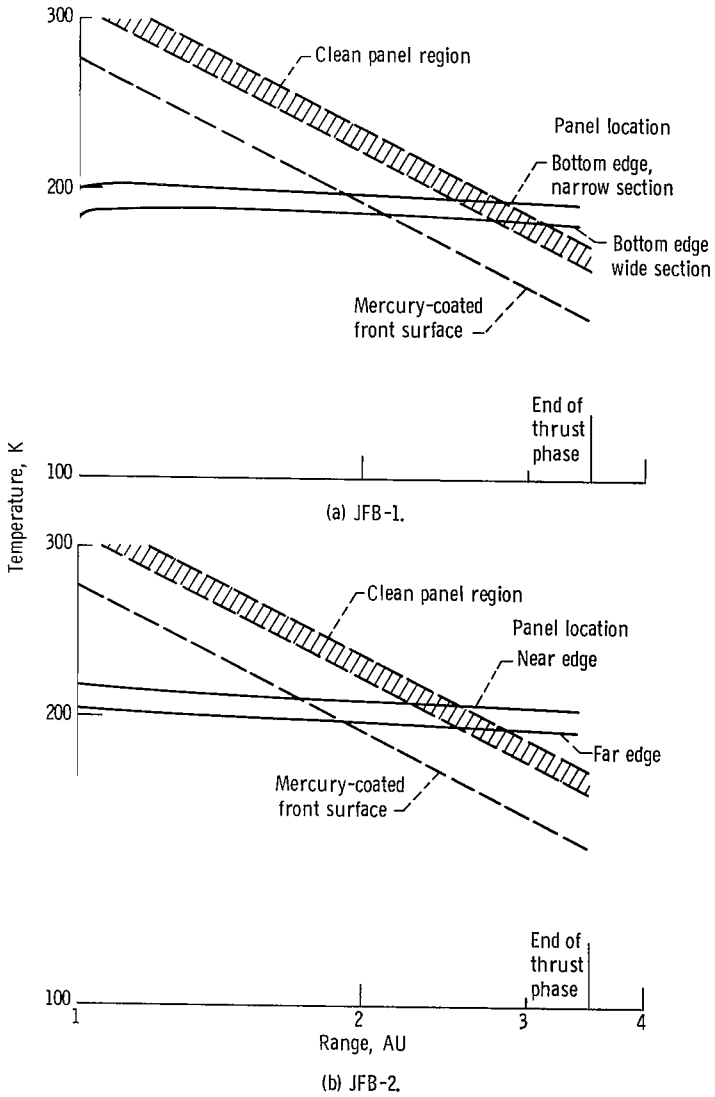

Figure 17. - Comparison of possible panel temperatures and condensation temperatures for JFB spacecraft solar panels during thrusting phase of mission.

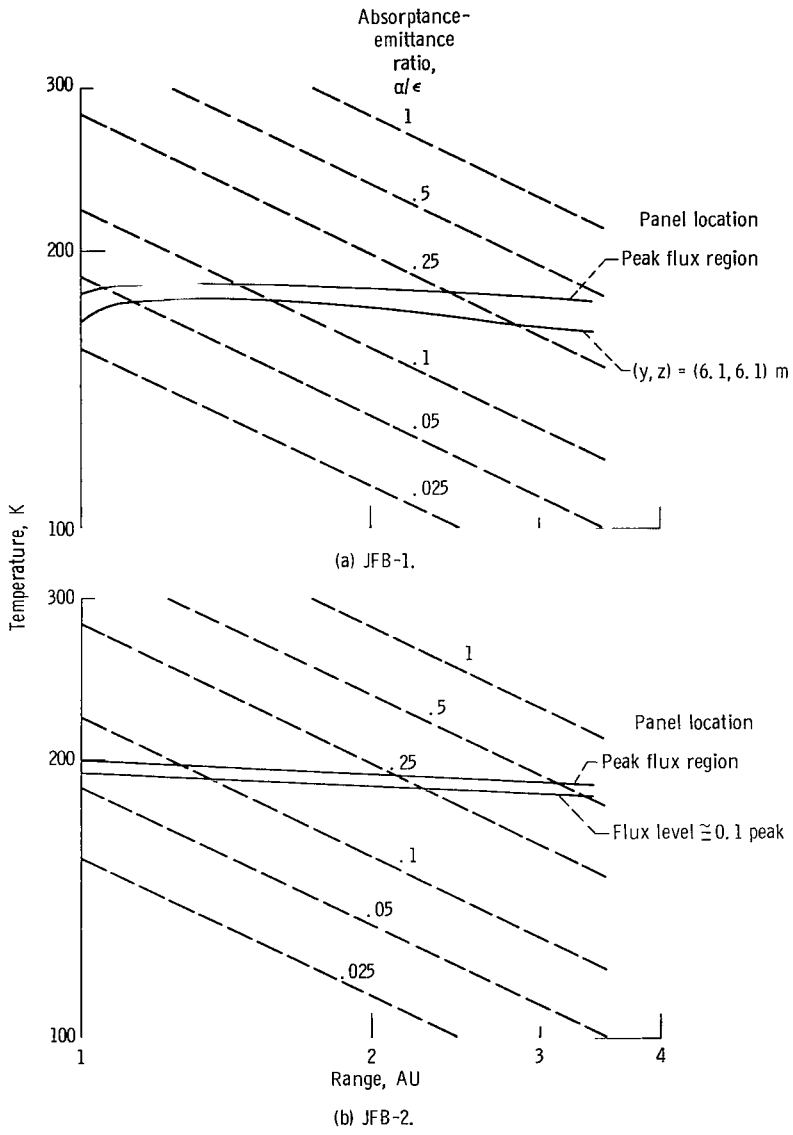

Figure 18. - Comparison of possible spacecraft temperatures with condensation temperatures for return flux rates at x = 0 plane during thrusting phase of mission.

NATIONAL AERONAUTICS AND SPACE ADMINISTRATION
WASHINGTON, D. C. 20546

OFFICIAL BUSINESS

FIRST CLASS MAIL

POSTAGE AND FEES P
NATIONAL AERONAUTIC
SPACE ADMINISTRATI

POSTMASTER: If Undeliverable (Section
Postal Manual) Do Not R

"The aeronautical and space activities of the United States shall be conducted so as to contribute . . . to the expansion of human knowledge of phenomena in the atmosphere and space. The Administration shall provide for the widest practicable and appropriate dissemination of information concerning its activities and the results thereof."

—NATIONAL AERONAUTICS AND SPACE ACT OF 1958

NASA SCIENTIFIC AND TECHNICAL PUBLICATIONS

TECHNICAL REPORTS: Scientific and technical information considered important, complete, and a lasting contribution to existing knowledge.

TECHNICAL NOTES: Information less broad in scope but nevertheless of importance as a contribution to existing knowledge.

TECHNICAL MEMORANDUMS: Information receiving limited distribution because of preliminary data, security classification, or other reasons.

CONTRACTOR REPORTS: Scientific and technical information generated under a NASA contract or grant and considered an important contribution to existing knowledge.

TECHNICAL TRANSLATIONS: Information published in a foreign language considered to merit NASA distribution in English.

SPECIAL PUBLICATIONS: Information derived from or of value to NASA activities. Publications include conference proceedings, monographs, data compilations, handbooks, sourcebooks, and special bibliographies.

TECHNOLOGY UTILIZATION PUBLICATIONS: Information on technology used by NASA that may be of particular interest in commercial and other non-aerospace applications. Publications include Tech Briefs, Technology Utilization Reports and Notes, and Technology Surveys.

Details on the availability of these publications may be obtained from:

SCIENTIFIC AND TECHNICAL INFORMATION DIVISION

NATIONAL AERONAUTICS AND SPACE ADMINISTRATION

Washington, D.C. 20546